Monte Carlo Trajectory Calculations of the Dissociation of HCl in Ar*

Ven H. Shui, John P. Appleton, and James C. Keck

Department of Mechanical Engineering, Massachusetts Institute of Technology, Cambridge, Massachusetts 02139

(Received 16 December 1971)

The modified phase–space theory of reaction rates is applied to the dissociation of HCl in a heat bath of argon atoms. Excellent agreement is obtained between the theoretical predictions and the shock-tube measurements of the dissociation rate coefficient over the temperature range 2500–5000°K. The recrossing correction factor and nonequilibrium correction factor are obtained from Monte Carlo trajectory calculations for states near the dissociation limit. The trajectories were sampled within the reaction zone, with a weight proportional to the equilibrium reaction rate, and numerically integrated in both time-wise directions to determine the complete histories of the collisions. A simple separable function for the equilibrium transition rate $R(\epsilon_i, \epsilon_f)$ from initial states ϵ_i to final states ϵ_f was obtained to fit the numerical data with sufficient accuracy and was used to solve the steady-state master equation. Important features of collisions of highly asymmetric diatomic molecules are discussed, and several typical reactive trajectories are shown to illustrate the importance of rotational motion is such collisions.

I. INTRODUCTION

The modified phase-space theory of reaction rates has been developed by Keck and his co-workers[1–5] and applied quite successfully to the three-body recombination and dissociation of diatomic molecules which have similar atomic masses. However, as demonstrated by Shui, Appleton, and Keck,[4] the theoretical predictions of the dissociation rate coefficients k_d for HF and HCl are much too low by comparison with experimental measurements (see Figs. 9 and 10 of Ref. 4), although the barrier rate coefficients $k_d{}^B$ lie above the experimental measurements and have about the right temperature dependence. The reason for this disagreement was believed to be that the estimates of the recrossing correction factors $(N/N_0) \lesssim 0.01$, and the nonequilibrium correction factors $(k/k_e) \simeq 0.01$ were too small.

The correlation formulas used in Ref. 4 to estimate the values of (N/N_0) and (k/k_e) were deduced using the results of Monte Carlo trajectory calculations[6] and master equation solutions[7] in which the recombining (dissociating) molecules had atoms of similar masses. It was suggested[4] that the mechanics of reacting collision processes in which one of the recombining atoms had a very small mass, such as the hydrogen halides, was sufficiently different from those cases considered in Refs. 6 and 7, that the correlation formulas were no longer valid.

This paper presents results of Monte Carlo trajectory calculations for the HCl+Ar system, and from these, determinations were made of the dissociation rate coefficients which could be compared with shock-tube measurements. In Sec. II the equations and statistical methods used to obtain the numerical results are derived and summarized. Section III presents a summary of the results and their comparison with the experimental measurements, and Sec. IV contains our concluding discussion.

II. MONTE CARLO TRAJECTORY CALCULATIONS

The steady state reaction rate coefficient k (subscript r for recombination; d for dissociation) is given by the relationship

$$k = k^B (N/N_0)(k/k_e), \qquad (2.1)$$

where the "barrier" rate coefficient k^B is defined as

$$k^B = \mathfrak{R}_v(0)/V \prod_j [M_j]. \qquad (2.2)$$

In Eq. (2.2), V is the normalization volume in configuration space, $[M_j]$ is the concentration of particles of type M_j in the initial state,

$$\mathfrak{R}_v(\epsilon) = \int_{S(\epsilon)} \rho(\mathbf{v} \cdot \mathbf{n}) ds \qquad (2.3)$$

is the "variational rate" (see Ref. 2) for the surface $S(\epsilon)$ defined by

$$(H - B)/kT = \epsilon, \qquad (2.4)$$

and the corresponding equilibrium one-way crossing rate $\mathfrak{R}(\epsilon)$ is given by the expression

$$\mathfrak{R}(\epsilon) = (N/N_0) \cdot \mathfrak{R}_v(\epsilon). \qquad (2.5)$$

Here, ρ is the density of the representative points, $\mathbf{v}$ is the generalized velocity, $\mathbf{n}$ is the unit outward normal to ds, and B and H are the barrier height and Hamiltonian of the molecule, respectively. As implied by Eq. (2.4), the energy (ϵ) of the molecule is measured from the top of the rotational barrier. Other definitions and more detailed descriptions can be found in Refs. 2 and 3.

Monte Carlo trajectory calculations as applied here efficiently evaluate the correction factors (N/N_0) and (k/k_e) by statistically sampling within the reaction zone and numerically integrating the classical equations of motion in both time-wise directions to determine the complete history of the collisions. By sampling with a weight proportional to the local flow rate $\rho(\mathbf{v} \cdot \mathbf{n})$

4266

across the surface $S(\epsilon)$, a statistical distribution of trajectories is obtained which reflects their *a priori* contribution to the reaction rate, thus enabling calculations to be made of the correction factors without further weighting. The representative points were selected from the reaction zone region, i.e., on the surface $S(\epsilon)$, and the equations of motion were integrated outwards in both timewise directions and terminated as soon as the interaction with the third body became negligible. This avoided unnecessary integrations in regions where interactions were very weak and inconsequential to the outcome of the collisions.

A. Recrossing Correction Factor

The N_0 trajectories sampled which cross the barrier surface, $\epsilon = 0$, can be divided into four categories, i.e., $f \rightarrow b$, $f \rightarrow f$, $b \rightarrow b$, and $b \rightarrow f$, depending on whether the initial and final states of the molecule are free (f) or bound (b). The $f \rightarrow b$ trajectories are "reactive" (in terms of recombination) while the others are all regarded as being "nonreactive." The recrossing correction factor (N/N_0) is then given by the expression[6]

$$N/N_0 = \sum_n [N(f \mid n \mid b)/n]/N_0, \qquad (2.6)$$

where N is the effective number of reactive trajectories and $N(f \mid n \mid b)$ is the number of trajectories that go from a free state f to a bound state b with n crossings of the barrier surface in the direction $f \rightarrow b$, and $n-1$ crossings in the direction $b \rightarrow f$.

B. Transition Rates and Nonequilibrium Correction Factors

The nonequilibrium correction factor (k/k_e) is the ratio between the steady state reaction rate and the corresponding equilibrium reaction rate coefficient. Keck and Carrier[7] investigated the coupled vibration-dissociation–recombination process for gas mixtures which consisted primarily of diatomic molecules highly diluted in a heat bath of inert gas atoms such as argon. They presented techniques for solving the appropriate master equations and showed that great simplifications could be obtained if the kernel $R(\epsilon_i, \epsilon_f)$ in the master equation was separable. The kernel $R(\epsilon_i, \epsilon_f)$ is the "one-way" equilibrium transition rate between energy states $\epsilon = \epsilon_i$, and $\epsilon = \epsilon_f$, per unit volume, per unit initial and final energies. The energies are measured in the units of kT.

Monte Carlo trajectory calculations were first used to generate a relative numerical distribution of $R(\epsilon_i, \epsilon_f)$ as a function of ϵ_i and ϵ_f. A functional form for $R(\epsilon_i, \epsilon_f)$ was then obtained by a suitable fitting procedure which approximated the numerical distribution. This functional form was used, following Keck and Carrier's analysis,[7] to solve the appropriate master equation and

thus to obtain the corresponding nonequilibrium correction factors k/k_e.

The method of generating the relative numerical distributions of $R(\epsilon_i, \epsilon_f)$ from Monte Carlo trajectory calculations employed was similar to that used by Mansbach and Keck[8] which they applied to the problem of atomic excitation and ionization by thermal electrons. Briefly, samples were taken from surfaces within a few kT below the rotational barrier (e.g., $\epsilon = -1, -2, -3$) in addition to the samples taken on the barrier surface ($\epsilon = 0$). The reactive trajectories, i.e., $f \rightarrow b$, were divided into groups or "boxes," according to the magnitude of ϵ_i and ϵ_f, and the effective number of reactive trajectories in each box was then counted. The equilibrium transition rate is given by

$$R(\epsilon_i, \epsilon_f) = [f_k(\epsilon)/(\Delta\epsilon)^2] \cdot \mathcal{R}_v(\epsilon), \qquad (2.7)$$

where $(\Delta\epsilon)^2$ is the size of the box, ϵ is the position of the surface from which samples were taken, the subscript k specifies the box defined by ϵ_i, ϵ_f, and $(\Delta\epsilon)^2$, and

$$f_k(\epsilon) = \sum_{i=1}^{N_0} (x_{jk}/n_j)/N_0(\epsilon) \qquad (2.8)$$

is the effective number of reactive trajectories falling in the kth box. Here, $x_{jk} = 1$ if the trajectory is reactive, $x_{jk} = 0$ if it is nonreactive, and n_j is the number of crossings of that trajectory in the reactive direction (e.g., from free to bound, in the case of recombination).

As was observed previously, a separable form of the kernel $R(\epsilon_i, \epsilon_f)$ results in great simplification in solving the master equations. We found that the empirical form

$$R(\epsilon_i, \epsilon_f) = AG(\epsilon_f) \exp(\alpha\epsilon_f - \beta\epsilon_i) \qquad (2.9)$$

was able to reproduce the relative numerical distribution of $R(\epsilon_i, \epsilon_f)$ with sufficient accuracy. In Eq. (2.9) A, α, and β are constants and $G(\epsilon_f)$ is a relatively slowly varying function.

It was observed from the map of the relative numerical distribution of $R(\epsilon_i, \epsilon_f)$ that the kernel exhibits a sharp maximum along the diagonal $\epsilon_i = \epsilon_f$, dies off very rapidly away from the diagonal, and varies relatively slowly along the diagonal. Thus the fitting was made easier by rotating the energy coordinates and expressing the kernel in the form $R(\Delta, \bar{\epsilon})$, where

$$\Delta = |\epsilon_i - \epsilon_f| \qquad (2.10a)$$

is the absolute value of the energy transfer and

$$\bar{\epsilon} = (\epsilon_i + \epsilon_f)/2 \qquad (2.10b)$$

is the mean of the initial and final energies. The symmetry of $R(\epsilon_i, \epsilon_f)$ in ϵ_i and ϵ_f requires that

$$R(\epsilon_i, \epsilon_f) = R(\Delta, \bar{\epsilon}). \qquad (2.11)$$

Thus, in view of the kernel's rapid decay with Δ and the fact that the function $G(\epsilon_f)$ is relatively slowly

varying, we can write

$$R(\Delta, \bar{\epsilon}) = AG(\bar{\epsilon}) \exp(-a\Delta - b\bar{\epsilon}) \qquad (2.12)$$

with

$$\alpha = a - b/2, \quad \text{and} \quad \beta = a + b/2. \qquad (2.13)$$

Various moment of the energy transfer with respect to the kernel were used in the fitting procedure (see also Sec. III.B). The mth moment of energy transfer $(\epsilon_i - \epsilon_f)$ with respect to $R(\epsilon_i, \epsilon_f)/\mathfrak{R}_v(\epsilon)$ is defined as

$$K_m(\epsilon) = \int_{-\infty}^{\epsilon} d\epsilon_f \int_{\epsilon}^{\infty} d\epsilon_i \left[\frac{R(\epsilon_i, \epsilon_f)}{\mathfrak{R}_v(\epsilon)} \right] (\epsilon_i - \epsilon_f)^{m-1}. \quad (2.14)$$

By substituting Eqs. (2.7) and (2.8) into Eq. (2.14) and evaluating the integral by Monte Carlo methods, we obtain

$$K_m(\epsilon) = \sum_{j=1}^{N_0} \left(\frac{x_j}{n_j} \right) \frac{(\epsilon_i - \epsilon_f)_j^{m-1}}{N_0(\epsilon)}, \qquad (2.15)$$

where $x_j = 1$ if the trajectory is reactive, and $x_j = 0$ otherwise. This is the equation used in the actual calculation of the moments $K_m(\epsilon)$ from data generated by trajectory calculations.

Now, the equilibrium one-way crossing rate $\mathfrak{R}(\epsilon)$ is defined as

$$\mathfrak{R}(\epsilon) \equiv \int_{-\infty}^{\epsilon} d\epsilon_f \int_{\epsilon}^{\infty} d\epsilon_i R(\epsilon_i, \epsilon_f). \qquad (2.16)$$

Rotating the energy coordinates to $[\Delta, \bar{\epsilon}]$ and using Eq. (2.12), we obtain

$$\mathfrak{R}(\epsilon) \approx AG(\epsilon) \exp(-b\epsilon)/(a^2 - b^2/4), \qquad (2.17)$$

where $G(\bar{\epsilon})$ has been expanded about ϵ and small terms dropped.

In addition, we found by plotting (N/N_0) versus ϵ, that the form

$$N(\epsilon)/N_0(\epsilon) = C \exp(p\epsilon) \qquad (2.18)$$

with both C and p constant, correlates the numerical data reasonably well. By combining Eqs. (2.5), (2.17), and (2.18), we obtain

$$\mathfrak{R}_v(\epsilon) \exp(\epsilon)/\mathfrak{R}_v(0) = G(\epsilon), \qquad (2.19)$$

$$b = 1 - p, \qquad (2.20)$$

and

$$A/\mathfrak{R}_v(0) = C(a^2 - b^2/4). \qquad (2.21)$$

The moments defined by Eq. (2.14) can then be evaluated by using the above relationships as follows:

$$K_m(\epsilon) = A[G(\epsilon) \exp(-\epsilon)\mathfrak{R}_v(0)]^{-1}$$
$$\times \int_{\epsilon - \Delta/2}^{\epsilon + \Delta/2} d\bar{\epsilon} \int_0^{\infty} d\Delta G(\bar{\epsilon}) \exp(-a\Delta - b\bar{\epsilon}) \Delta^{m-1}. \quad (2.22)$$

When $a \gg b/2$, a good approximation is

$$K_m(\epsilon) \approx Cm! a^{1-m} \exp[(1-b)\epsilon]. \qquad (2.23)$$

The ratios of these moments are independent of the energy ϵ, and the parameter a may be obtained directly

from any of these ratios. However, since we anticipate from the diffusion analysis[7] that it is the first and the second moments which are most important for determining the steady-state rate coefficients, we have used the value of a given by the ratio $2K_1/K_2$.

Having obtained a separable form for the transition kernel, we can now proceed to solve the steady-state master equations which will yield the nonequilibrium correction factor. Keck and Carrier[7] showed that the steady-state master equation can be transformed exactly into an equivalent diffusion equation and then solved subject to the appropriate boundary conditions. For the case of the separable kernel, they assumed

$$R(\epsilon_i, \epsilon_f) = r_2(\epsilon_i) r_1(\epsilon_f); \qquad \epsilon_i > \epsilon_f,$$
$$= r_2(\epsilon_f) r_1(\epsilon_i); \qquad \epsilon_f > \epsilon_i, \qquad (2.24)$$

and

$$R(c, \epsilon) = r_1(\epsilon) r_c, \qquad (2.25)$$

where r_c is a constant and

$$R(c, \epsilon) = \int_0^{\infty} R(\epsilon', \epsilon) d\epsilon' \qquad (2.26)$$

is the equilibrium recombination (or dissociation) rate.

By solving the equivalent diffusion equation, they obtained the expression for the nonequilibrium correction factor

$$\frac{k}{k_e} = \left[\mathfrak{R}(0) \left(\int_{-\delta}^0 WZ^{-2} d\epsilon + \frac{r_2(0)}{r_c Z(0)} \right) \right]^{-1} \quad (2.27)$$

where $\mathfrak{R}(0)$ is the one-way equilibrium flux of molecules across the energy surface $\epsilon = 0$, defined in Eq. (2.16), and

$$W(\epsilon) = r_2(dr_1/d\epsilon) - r_1(dr_2/d\epsilon) \qquad (2.28)$$

is the Wronskian of r_2 and r_1, and

$$Z(\epsilon) = r_2(\epsilon) \int_{-\delta}^{\epsilon} r_1(\epsilon') d\epsilon' + r_1(\epsilon) \left(\int_{\epsilon}^0 r_2(\epsilon') d\epsilon' + r_c \right) \quad (2.29)$$

is the equilibrium collision rate, and $\delta = D/kT$ is the dimensionless potential-well depth of the molecule.

Since we sampled trajectories for recombination, the condition, $\epsilon_i > \epsilon_f$, was satisfied in all cases. Thus, for the kernel given by Eq. (2.9), we have

$$r_2(\epsilon_i) = \exp(-\beta\epsilon_i), \qquad r_1(\epsilon_f) = AG(\epsilon_f) \exp(\alpha\epsilon_f) \quad (2.30)$$

and

$$r_c = 1/\beta. \qquad (2.31)$$

By substituting Eqs. (2.34) and (2.35) into Eqs. (2.32) and (2.33) and then into Eq. (2.31), we obtain

$$k/k_e \approx [1 - (\alpha/\beta)^2][G(\epsilon^*)/G(0)], \qquad (2.32)$$

where ϵ^* is the location of the maximum of $G(\epsilon) \exp(-b\epsilon)$.

III. RESULTS

A. The Interaction Potential

A Morse potential function is used to describe the two-body interaction between H and Cl as before,[4] with the same potential parameters; i.e., $D=4.62$ eV (53 600 °K), $r_e=1.275$ Å, and $\beta=1.87$ Å^{-1}. However, dumb-bell models as used before[3,6] for the three-body interaction potential are not well defined when V_{XM} and V_{YM} are considerably different and have attractive potential wells. To overcome this difficulty, we reverted to the use of the purely repulsive Mason–Vanderslice exponential interaction potential,[1,7,9]

$$V=A\,\exp(-r/l). \qquad (3.1)$$

Then the dumbbell model is defined as

$$V_3=V_{XM} \quad \text{for} \quad V_{XM}>V_{YM},$$

and

$$V_3=V_{YM} \quad \text{for} \quad V_{XM}<V_{YM}. \qquad (3.2)$$

This change should not affect the results which are of concern here since we consider only dissociation rate

TABLE I. Mason–Vanderslice potential parameters.

System	A (eV)	l (Å)
Ar+H	268	0.35
Ar+Cl	1060	0.35

measurements at high temperatures (2500–5000 °K), and it has been shown[3-5] that the potential well in V_3 has negligible effects on reaction rate coefficients at such elevated temperatures. Table I summarizes the parameters A_{iM} and l_{iM} used in the present calculations.

B. Reaction Rates

Table II shows the distribution of the three hundred trajectories sampled for the case of Ar+HCl at 2500°K ($kT/D=0.0466$) with $\epsilon=0$, classified according to the nature of their end states (see Sec. II.A). The implications of Table II have already been discussed by Keck.[6] Of course, as pointed out before, his empirical correlation formula for (N/N_0) does not apply to the present case. In addition, Keck's Table I for homonuclear molecules showed entries of comparable magnitude for $N(f\mid n\mid f)$ and $N(b\mid n\mid b)$; whereas, we found that $N(f\mid n\mid f)\gg N(b\mid n\mid b)$ for Ar+HCl. The reason for this difference will be explained in Sec. IV when we discuss details of the Ar+HCl trajectories.

The recrossing correction factor N/N_0 for the various temperatures and surfaces sampled are plotted versus ϵ in Fig. 1. No definite temperature dependence can be determined from the plot (Keck's previous results[2,6] also did not show any temperature effect on N/N_0).

TABLE II. Distribution of trajectories with respect to class of reaction and number of traversals of the barrier surface ($\epsilon=0$), for Ar+HCl at 2500°K ($kT/D=0.047$).

Class		N			
	n	1	2	3	Total
$(f\mid n\mid b)$		91	8		99
$(f\mid n\mid f)$		142	9	2	153
$(b\mid n\mid b)$		10	4		14
$(b\mid n\mid f)$		16	2		18
Total					284

Recrossing correction factor $(N/N_0)=(91+8/2)/284=0.33$

Although there is considerable scatter in the data, the least-squares fit line does give a reasonable representation of all the data points. The parameters $p=0.26$, $b=1-p=0.74$, and $C=[N(0)/N_0(0)]=0.27$ are all obtained from this fitted line [see Eqs. (2.19) and (2.21)].

The various moments $K_m(\epsilon)$, as defined by Eq. (2.14), were then calculated using Eq. (2.15) and tabulated in Table III. The ratio $2K_1/K_2\approx a$ [see Eqs. (2.26) and (2.27)] is also included in the table.

In order to complete the determination of the transition kernel $R(\epsilon_i,\,\epsilon_f)$ and produce a map of its relative numerical distribution, we must first find the pre-exponential function $G(\epsilon_f)$ (see Sec. II.B). Keck[2] found that the function

$$G(\epsilon)=[1-(-\epsilon/\delta)^{1/2}]/[1+(-\epsilon/\delta)^{1/2}] \qquad (3.3)$$

was able to represent his numerical calculations of $\mathfrak{R}_v(\epsilon)/\mathfrak{R}_v(0)$ with sufficient accuracy, and we have

TABLE III. Moments $[K_m(\epsilon)]$ for Ar+HCl.

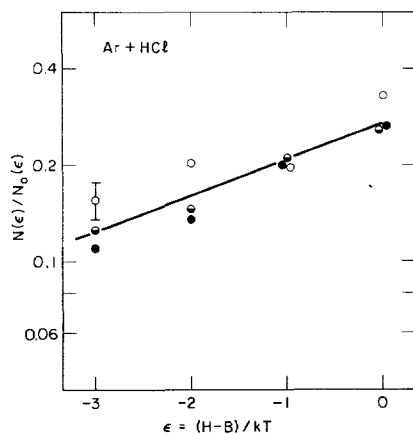| T (°K)	kT/D	ϵ	K_0	K_1	K_2	$2K_1/K_2$
5000	0.093	0	1.09	0.245	0.159	3.08
		−1	0.501	0.182	0.158	2.30
		−2	0.505	0.102	0.079	2.58
		−3	0.348	0.080	0.043	3.72
		mean				2.92
3500	0.065	0	1.34	0.233	0.174	2.68
		−1	0.693	0.190	0.242	1.57
		−2	0.321	0.130	0.130	2.00
		−3	0.464	0.112	0.095	2.36
		mean				2.15
2500	0.047	0	1.71	0.331	0.332	1.99
		−1	0.675	0.192	0.247	1.56
		−2	0.555	0.202	0.241	1.68
		−3	0.364	0.157	0.162	1.94
		mean				1.79

FIG. 1. Recrossing correction factors N/N_0 versus energy of the surface from which samples were taken. ●, $T=5000°K$; ◖, $T=3500°K$; ○, $T=2500°K$. Solid line is the best least-squares fit for all points. The slope of this line determines the parameter b.

used this form for $G(\epsilon_f)$. The resulting numerical distribution of $R(\epsilon_i, \epsilon_f)/\mathfrak{R}_v(0)$ is shown in Fig. 2, again for Ar+HCl at 2500 °K. The figures in the boxes represent the mean value of $R(\epsilon_i, \epsilon_f)/\mathfrak{R}_v(0)$ for the box. Because of the sampling technique employed each value of ϵ used in the calculations gives data in a quadrant that touches the diagonal $\epsilon_i=\epsilon_f$, at a value of $(\epsilon_i+\epsilon_f)/2=\bar{\epsilon}=\epsilon$. Data in overlapping quadrants agreed within the statistical errors and were averaged to obtain the results shown. The total number of trajectories sampled was approximately three hundred for each value of $\epsilon(\epsilon=0, -1, -2, -3)$. The results shown were calculated for $\epsilon_i>\epsilon_f$ (recombination); however, since $R(\epsilon_i, \epsilon_f)$ is symmetrical in ϵ_i and ϵ_f, the values for $\epsilon_i<\epsilon_f$, may be obtained by reflection in the diagonal $\epsilon_i=\epsilon_f$. As was pointed out in Section II.B, the map shows that $R(\epsilon_i, \epsilon_f)$ exhibits a sharp maximum ridge along $\epsilon_i=\epsilon_f$, which corresponds to zero energy transfer; this dies off rapidly as $|\epsilon_i-\epsilon_f|$ increases. Combining Eqs. (2.9) and (2.21), we obtain

$$R(\epsilon_i, \epsilon_f)/\mathfrak{R}_v(0) = C(a^2-b^2/4)G(\epsilon_f)\exp(\alpha\epsilon_f-\beta\epsilon_i).$$

$$(3.4)$$

Since all the parameters in Eq. (3.2) have been obtained, we can use them to generate the function $R(\epsilon_i, \epsilon_f)/\mathfrak{R}_v(0)$. The parameter a used is the average of the four values of $2K_1/K_2$ in Table III. The result

TABLE IV. Dissociation rate coefficients for Ar+HCl.

$T(°K)$	kT/D	$k_d{}^B$	N/N_0	b	a	k/k_e	k_d
5000	0.093	5.69^{-13}	0.27	0.74	2.92	0.30	4.55^{-14}
3500	0.065	7.26^{-15}	0.27	0.74	2.15	0.42	8.27^{-16}
2500	0.047	1.81^{-17}	0.27	0.74	1.79	0.50	2.44^{-18}

$k_d{}^B$ and k_d have units cm³ molecule⁻¹·sec⁻¹.

for $T=2500$ °K is plotted in the upper left corner of Fig. 2 as a contour map. We see that this map reproduces all the important features of the actual distribution, and the agreement in general is very good.

In Fig. 3 we have plotted $[R(\Delta, \bar{\epsilon})/\mathfrak{R}_v(0)]/[\mathfrak{R}(\bar{\epsilon})/\mathfrak{R}(0)]$ versus Δ. The factor $[\mathfrak{R}(\bar{\epsilon})/\mathfrak{R}(0)]$ is included for normalization purposes. The solid line passing through the bulk of the data points has a slope, $a=1.79$, as determined above (see Table III). It can be seen that for $\Delta<0.5$, the data points deviate con-
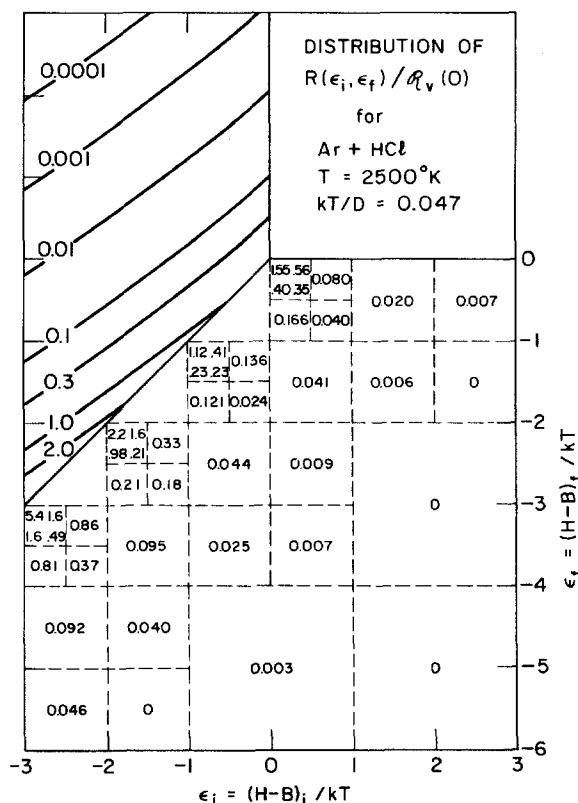

FIG. 2. Map of numerical distribution of the function $R(\epsilon_i, \epsilon_f)/\mathfrak{R}_v(0)$, where $R(\epsilon_i, \epsilon_f)$ is the equilibrium transition rate and $\mathfrak{R}_v(0)$ is the variational rate for the surface $\epsilon=0$. The contour map, calculated from Eq. (3.2) using the fitted parameters, is plotted in the upper left corner to avoid overcrowding the figure. Comparison may be done by reflection through the diagonal $\epsilon_i=\epsilon_f$.

siderably from this line; however, the region around $\Delta\approx1$, has the most important contribution in the determination of the nonequilibrium correction factor, and the line fits the data very well in this region.

We therefore conclude that our functional form for $R(\epsilon_i, \epsilon_f)$ and the associated parameters determined above lead to a very good representation of the transition kernel. At the same time, it is still simple enough so that the steady-state master equation can be solved analytically without the usual reliance on a great deal of numerical computation.

The nonequilibrium correction factors may now be calculated from Eqs. (2.13) and (2.36). The barrier

rate coefficients are taken from Ref. 4 and the results are summarized in Table IV for $T = 5000$, 3500, and 2500 °K. It should be noted that for the results shown, the corresponding characteristic energy transfer in a collision is between $0.4kT$ and $0.6kT$. The statistical errors, based on one standard deviation, are estimated to be about 10% for (N/N_0) and 20% for (k/k_e).

Figure 4 is an Arrhenius plot of the measured (full lines and open points) and calculated (solid points) dissociation rate coefficients of HCl in Ar. It shows that the present theoretical predictions are in excellent agreement both in terms of magnitude and temperature dependence with the experimental measurements of Seery and Bowman,[10] Fishburne,[11] and Jacobs, Cohen, and Giedt.[12] We should point out that the major temperature dependence of k_d is determined by the barrier rate coefficient k_d^B. The correction factors (N/N_0) and (k/k_e) lower the rates and introduce an additional relatively weak temperature dependence to the rate coefficients. Error bars on the theoretical points show estimated statistical errors of $\pm 20\%$.

IV. DISCUSSION

The Landau–Teller theory of vibrational relaxation,[13] as extended by Schwartz, Slawsky, and Herzfeld (SSH),[14] which considered vibrational–translational
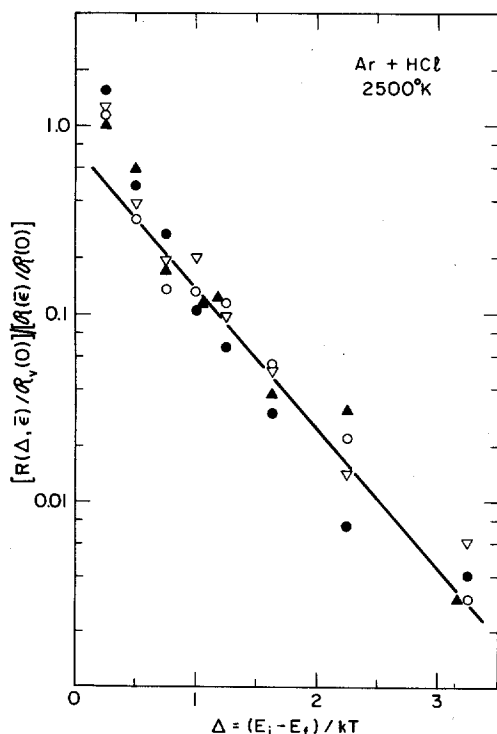

FIG. 4. Comparison between theoretical predictions of the dissociation rate coefficient and experimental measurements, as a function of T. ♦, theoretical predictions; O, Seery et al.; (F), Fishburne; (J), Jacobs et al.; dashed curve represents the theoretical barrier rate coefficients.

FIG. 3. The function $[R(\Delta, \bar{\epsilon})/\mathfrak{R}_v(0)]/[\mathfrak{R}(\bar{\epsilon})/\mathfrak{R}(0)]$ is plotted versus Δ, the absolute value of energy transfer. ●, $\bar{\epsilon} = 0$; O, $\bar{\epsilon} = -1$; ▲, $\bar{\epsilon} = -2$; ▽, $\bar{\epsilon} = -3$. The factor $[\mathfrak{R}(\bar{\epsilon})/\mathfrak{R}(0)]$ is included for normalization purposes so that the data can be better represented by a single line. The solid line which passes through the bulk of the data has a slope a taken from Table III. See text, Sec. III.B.
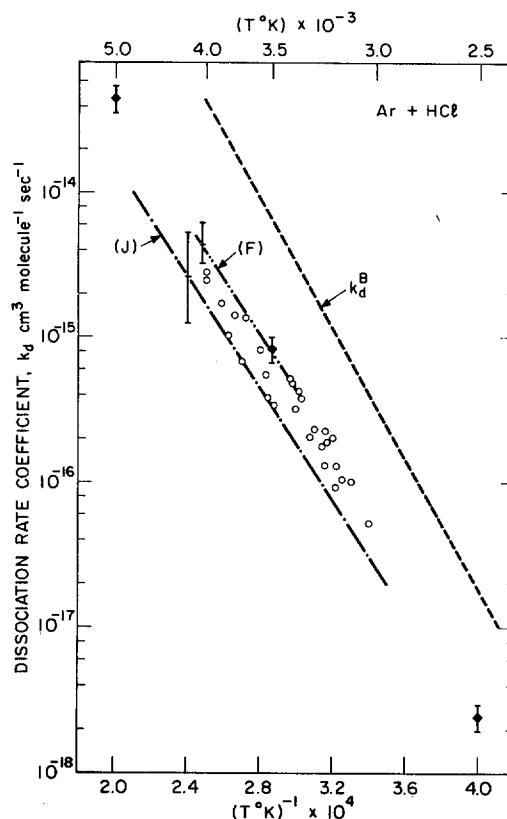
energy transfer, provided both a successful qualitative explanation and quantitative correlation of the vibrational relaxation rates of most of the homonuclear diatomic molecules which have been investigated. However, when applied to highly asymmetric heteronuclear diatomic molecules (e.g., HF and HCl), the theory predicted rates[15] several orders of magnitude slower than those observed experimentally.[16–20] This discrepancy led to the suspicion that rotational motion may be important in vibrational relaxation. Much work has been done in this respect, and it appears that by properly accounting for the rotational motion of the molecules, the very high vibrational relaxation rates for molecules such as HF and HCl, as well as the effects of deuteration, can now be explained and correlated. Detailed discussions and references on the topic of rotation–vibration coupling can be found in papers by Moore,[21] Chen and Moore,[22] and in a recent comment by Nikitin.[23]

According to the SSH theory, the efficiency of energy transfer for a collision depends on an "adiabaticity factor" $f(\omega\tau)$, where ω is the vibrational frequency of the molecule, and τ is the "effective time" of the collision, i.e., the time available for energy transfer. In the theory, the relative velocity between the *center*
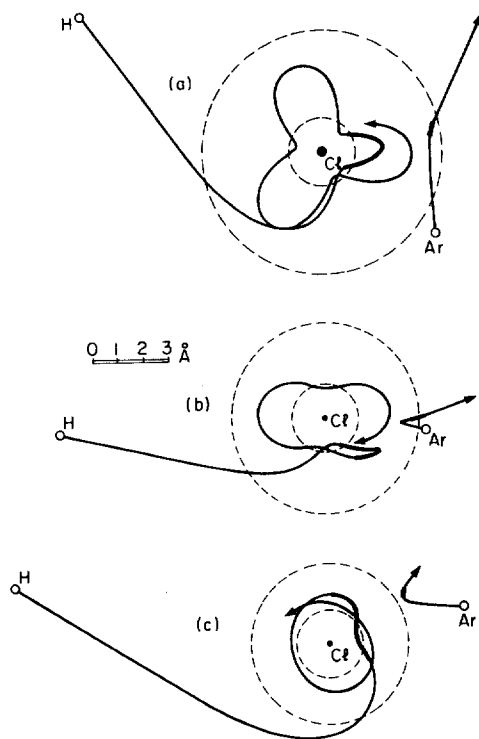
FIG. 5. Typical reactive trajectories. The thicker lines on the trajectories indicate zones of strong interaction.

of mass of the molecule and the collision partner is used to estimate τ; thus $\tau \alpha (\mu_{XY,M})^{1/2}$, where $\mu_{XY,M} = m_{XY}m_M/(m_{XY}+m_M)$ is the effective reduced mass of the collision complex. Such reasoning as this led Keck to seek a correlation of the recrossing correction factors (N/N_0) for homonuclear molecules and various collision partners on the basis of the adiabaticity parameter, $\omega\tau\alpha(\mu_{XY,M}/\mu_{XY})^{1/2}$. However, for such systems as HCl+Ar, the hydrogen atom moves much more rapidly than does either the Cl or Ar atoms due to its much lighter mass. As can be seen in the trajectories shown in Fig. 5, the essential motion of the H atom is that of rotation about the Cl atom. Thus a more correct collision time for these heteronuclear systems is determined by the motion of the H atom relative to the Ar atom and not by the relative motion of the HCl and Ar. Consequently, the quantity $\mu_{HCl,Ar}$ in the SSH theory should more properly be replaced by $\mu_{HAr}=m_H m_{Ar}/(m_H+m_{Ar})\approx m_H$, the reduced mass of the H–Ar collision. This point is clearly illustrated by the three reactive trajectories we plotted in Fig. 5. The duration of the strong interaction, where most of the energy and momentum transfers occur, is indicated by the thicker lines on the trajectories. We see that during this period of strong interaction (corresponding to the effective collision time), the Ar atom hardly moves relative to the Cl atom whereas, by rotation, the H atom passes completely through the reaction zone. Since the adiabaticity factor $f(\omega\tau)$ has a dependence

given by the factor $\exp(-\alpha\omega\tau)^\beta$, where both α and β are of order unity, the change from $\mu_{XY,M}$ to μ_{XM} increases the magnitude of the adiabaticity parameter to order unity for such systems as HCl+Ar and thus raises the calculated vibrational relaxation rates by several orders of magnitude in agreement with experimental observations. Additional trajectory calculations for the heteronuclear molecules using different collision partners are required before we are in a position to deduce correlation formulas for the correction factors similar to those obtained by Keck.

The inner dashed circles in Fig. 5 indicate the equilibrium separation for HCl molecules, the outer dashed circles are the positions z_2 of the rotational maximum evaluated at the end of the collision. In general the following observations can be made about the HCl–Ar collisions:

1. For nonreactive collisions (unlike those shown in Fig. 5) the Ar atom acts as a block which prevents the H atom from reaching the Cl atom by virtue of its position between the Cl and H atoms; i.e., $r_{HCl}>r_{HAr}$. These collisions are, in fact, automatically excluded from our samples since they never reach the reaction zone.

2. On the other hand, participation of Ar in the collision is necessary to take away the excess energy from H·Cl and thereby effect a recombination. Thus typical reactive trajectories, such as those shown in Fig. 5, may be divided into three different phases:

(i) The H atom approaches the Cl atom from the opposite side to the Ar atom with little or no interference from Ar.

(ii) Due to the action of the strong attractive valence forces between H and Cl, the H atom cuts into a line joining Ar and Cl and transfers energy and momentum to Ar. This is the zone of strong interaction (thicker line on the trajectories) during which most of the energy and momentum exchanges are effected. We note that at the beginning of this reaction zone, the Ar atom is usually very near the turning point with respect to the Cl atom so that its kinetic energy is very low.

(iii) The H atom, having lost sufficient energy, becomes bound to Cl atom and then proceeds to vibrate and rotate about the latter; whereas, the Ar atom moves away from HCl molecule with an increased velocity.

We should point out that for convenience of representation in two dimensions, the trajectories shown in Fig. 5 have all three particles moving in the same plane. However, our calculations were, in general, three dimensional.

In Sec. III.B we noted that $N(f \mid n \mid f) \gg N(b \mid n \mid b)$ for Ar+HCl collisions; whereas, Keck[6] obtained $N(f \mid n \mid f) \approx N(b \mid n \mid b)$ for all the homonuclear molecules he investigated. The reason for this difference can now be explained. The variational reaction rate calculations show that the contribution to the reaction rate from collisions with the Cl end of the

molecule is negligible. In addition, both Ar and Cl can be regarded as almost stationary while the hydrogen atom moves about at high average velocities. Therefore, most of the energy exchanges that may change the state of HCl must come from the H–Ar collision, with very little direct influence from the Cl atom. Our sampling procedure ensures that the molecule must be on the energy surface $H-B=0$ at a certain time $t=t_0$, and the trajectory must cross that surface at t_0 with a negative slope (for recombination); i.e., the molecule must be in a free state $(H-B>0)$ at some time $t<t_0$ and must be losing energy to the Ar atom. Consider the case in which the H atom was initially bound to the Cl atom at $t\ll t_0$. The result of the H+Ar collision would be either (a) a net loss of energy from H to Ar, with the HCl molecule remaining bound, or (b) a net gain of energy by H from Ar, making H free from Cl. Obviously trajectories (a) are not sampled by our procedure since they do not cross the surface $H-B=0$; nor do trajectories (b) cross the surface in the desired direction since, once the H atom becomes free *after* a collision with the Ar atom, its rapid motion will carry it away from the Cl+Ar system. Thus no further significant energy transfer between H and Ar, which would change the state of HCl, is probable; i.e., HCl remains free, and those trajectories are not sampled. On the other hand, it is easy to see that if H was initially free at $t\ll t_0$, its collision with Ar would produce $f\rightarrow b$ trajectories that satisfy our sampling requirements. Consequently, the result $N(f\mid n\mid f)\gg N(b\mid n\mid b)$ for Ar+HCl collisions is expected.

For homonuclear molecules, the outcome of case (b), above, may be quite different. The $b\rightarrow f$ transition would be a result of the collision between *one end* of the molecule and the third body, as before. However, rotation of the molecule may bring the *other end* into a collision with the third body and could thereby produce a $f\rightarrow b$ transition. These trajectories $(b\rightarrow f\rightarrow b)$ satisfy our sampling requirements, and $N(f\mid n\mid f)$ and $N(b\mid n\mid b)$ may therefore have comparable magnitudes. Typical trajectories of this kind which illustrates our point will be presented when we report our work on homonuclear molecules.

It should be noted that the features of the collision mechanics discussed above would be suppressed if only colinear collisions were considered. Thus the one-dimensional approximation sometimes used in theoretical analyses of this nature presents a picture which is very different from what actually is the case for both homonuclear and heteronuclear molecules.

For a collision to be reactive (consider recombination), the molecule must start in a free state and end in a bound state. The corresponding energy changes must be such that $H-B<0$, where H is the Hamiltonian of the molecule, and B is the height of the rotational barrier. Figure 6 shows a distribution plot of ΔH and ΔB for 101 reactive trajectories out of the 300 trajectories sampled for HCl+Ar at 2500 °K on the
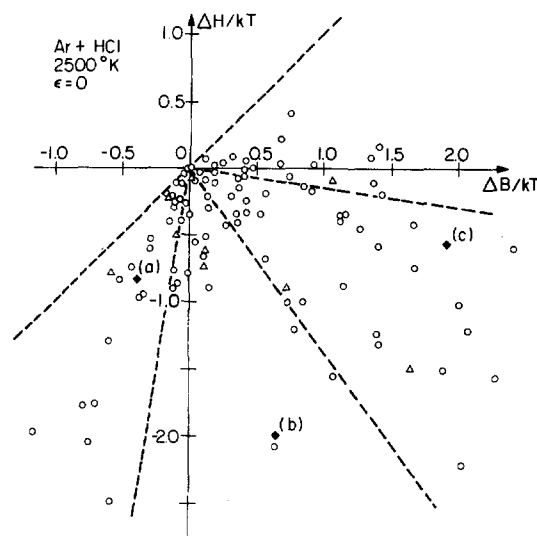

FIG. 6. Distribution plot of reactive trajectories in the $[\Delta H, \Delta B]$ plane. The average angular distribution and limits of one standard deviation are indicated by dashed lines.

surface $S(0)$. It is apparent that recombination (the change from $H-B>0$ to $H-B<0$) is achieved by two equally important mechanisms, i.e., reducing H and/or increasing B. Our work on homonuclear molecules (to be reported separately), on the other hand, shows that most recombinations are achieved by reducing H. This furnishes further evidence that rotational energy transfer in asymmetric molecules plays a relatively important part in chemical reactions. The energy transfers ΔH and ΔB for the three trajectories shown in Fig. 5 are indicated by the filled points in Fig. 6. They represent different ratios of $\Delta B/\Delta H$.

The calculations presented in this paper are for one system (Ar+HCl) and over a limited (high) temperature range (2500–5000°K). Work on other diatomic molecules is in progress which will cover the high-temperature dissociation region and the low-temperature recombination region. A number of interesting questions can be answered by such calculations; e.g., what is the physical interpretation of the parameters α and β involved in the equilibrium transition rates, and what will be the contribution from the "complex" mechanism to the overall recombination rate coefficient at low temperatures? In any event, the agreement between the theoretically predicted dissociation rate coefficients and experimental measurements for the case of HCl+Ar presented here undoubtedly provides another successful test for the classical modified phase–space theory of reaction rates.

¹ J. C. Keck, J. Chem. Phys. **32**, 1035 (1960).
² J. C. Keck, Advan. Chem. Phys. **13**, 85 (1967).
³ V. H. Shui, J. P. Appleton, and J. C. Keck, J. Chem. Phys. **53**, 2547 (1970).

[4] V. H. Shui, J. P. Appleton, and J. C. Keck, Symp. Combust. 13th, Salt Lake City, 1971, 19 (1972).
[5] V. H. Shui and J. P. Appleton, J. Chem. Phys. 55, 3126 (1971).
[6] J. C. Keck, Discussions Faraday Soc. 33, 173 (1962).
[7] J. C. Keck and G. F. Carrier, J. Chem. Phys. 43, 2284 (1965).
[8] P. Mansbach and J. C. Keck, Phys. Rev. 181, 275 (1969).
[9] E. A. Mason and J. T. Vanderslice, J. Chem. Phys. 28, 432 (1958).
[10] D. J. Seery and C. T. Bowman, J. Chem. Phys. 48, 4314 (1968).
[11] E. S. Fishburne, J. Chem. Phys. 45, 4053 (1966).
[12] (a) T. A. Jacobs, N. Cohen, and R. R. Giedt, J. Chem. Phys. 46, 1958 (1967). (b) R. R. Giedt and T. A. Jacobs, J. Chem. Phys. 55, 4144 (1971).
[13] L. Landau and E. Teller, Physik. Z. Sowjetunion 10, 34 (1936).

[14] (a) R. N. Schwartz, Z. I. Slawsky, and K. F. Herzfeld, J. Chem. Phys. 20, 1591 (1952). (b) R. N. Schwartz and K. R. Herzfeld, ibid. 22, 767 (1954).
[15] K. F. Herzfeld and T. A. Litovitz, Absorption and Dispersion of Ultrasonic Waves (Academic, New York, 1959).
[16] C. C. Chow and E. F. Green, J. Chem. Phys. 43, 324 (1965).
[17] W. D. Breshears and P. F. Bird, J. Chem. Phys. 50, 333 (1969).
[18] W. D. Breshears and P. F. Bird, J. Chem. Phys. 51, 3660 (1969).
[19] W. D. Breshears and P. F. Bird, J. Chem. Phys. 52, 999 (1970).
[20] J. R. Airey and S. F. Fried, Chem. Phys. Letters 8, 23 (1971).
[21] C. B. Moore, J. Chem. Phys. 43, 2979 (1965).
[22] H. L. Chen and C. B. Moore, J. Chem. Phys. 54, 4072 (1971).
[23] E. E. Nikitin, Comments At. Mol. Phys. 2, 59 (1970).

Phase Transitions Due to Softness of the Potential Core

G. STELL*

Department of Mechanics, State University of New York, Stony Brook, New York 11790

AND

P. C. HEMMER

Institute of Theoretical Physics, NTH, Trondheim, Norway

(Received 22 January 1971)

This paper extends a previous demonstration [Hemmer and Stell, Phys. Rev. Letters 24, 1284 (1970)] showing that for a system in which the pair potential has a hard core plus a negative part, softening the hard core can produce a second transition if a first already exists. Detailed analytic and numerical results for one-dimensional continuum fluids are given, and our discussion of the lattice gas is further developed. In particular interactions that are repulsive over next-nearest neighbor cells as well as nearest-neighbor cells are considered, and it is rigorously shown that as many as four first-order phase transitions can occur for such potentials, even in one dimension. The relevance of our work to certain features found in real systems (e.g. the possible breakdown of the law of rectilinear diameters, and isostructural solid–solid transitions) is also discussed, as is the novel critical behavior to be expected of certain two- and three-dimensional lattice systems.

I. INTRODUCTION

In a previous note[1] we showed that for a system in which the pair potential has a hard core plus a negative part, softening the hard core can produce a second transition if a first has already occured. Our demonstration consisted of a general plausibility argument for the occurrence of the second transition in lattice gases, plus explicit computations verifying that the second transition (and further transitions) can be induced in one-dimensional continuum fluids by softening the potential core. In this paper we extend and elaborate our earlier work.

Section II contains detailed results, both analytic and numerical, for one-dimensional fluids with nearest-neighbor repulsion and weak long-range attraction.

In Sec. III we augment the general plausibility arguments of Ref. 1. In particular we extend our discussion to the case in which the positive pair poten-tial acts on next-nearest neighbor particles as well as on neighboring particles, and we rigorously compute the ground-state energy for such a system in one dimension. The plausibility argument and the exact computation give compatible results; they show that in one dimension as many as four separate transitions occur for certain values of the strength parameters of the potential. We also discuss the new features that one should be prepared to meet as the dimensionality is increased, and we speculate on the possible existence of a novel form of tricritical point for $\nu \geq 2$.

In Sec. IV we note the relevance of our results to the general problem of formulating thermodynamic homogeneity assumptions (in the sense of Widom[2]) in a way that takes due account of the lack of exact symmetry in a fluid about its critical density ρ_c. We also briefly discuss the possibility that our work is pertinent to solid–solid transitions that preserve crystalline symmetry, such as are found experimentally in Ce and Cs.